Faculty of Natural and Applied Sciences Journal of Applied and Physical Sciences
Print ISSN: 3026-9857
www.fnasjournals.com
Volume 2; Issue 3; May 2025; Page No. 77-87.
DOI: https://doi.org/10.63561/japs.v2i3.816

Analysis of Radiative Heat Transfer Changes in the Flow Dynamics of Maxwell and Casson Nanofluids over a Vertically Aligned Plate with Internal Heat Generation

***[1]Jacob, E., [2]Adamu, M.A., [3]Aliyu, Z., & [4]Ogba, P.**
[1]Kogi State Polytechnic, Lokoja, Department of Statistics.
[2]Department of Metallurgical and Materials Engineering Technology, Kogi State Polytechnic, Lokoja.
[3]Department of Strategic Information, National Aids and STI Program, Federal Ministry of Health.
[4]Kogi State Polytechnic Lokoja, Department of Computer Science.

***Corresponding author email:** jacobemma001@gmail.com

Abstract
This study presents a comprehensive numerical investigation of radiative heat transfer and flow dynamics involving Maxwell and Casson nanofluids flowing past a vertically aligned plate, incorporating the effects of internal heat generation. These non-Newtonian fluids exhibiting memory and yield stress behaviors are examined to understand their influence on velocity, temperature, and concentration profiles under coupled thermal and solutal gradients. The governing partial differential equations representing momentum, energy, and mass conservation are transformed into coupled nonlinear ordinary differential equations using similarity variables. These are solved using the fourth-order Runge-Kutta method with a MATLAB-based shooting technique. Key dimensionless parameters such as the Prandtl number, Grashof number, Biot number, heat source parameter, Nusselt number, Sherwood number, and skin friction coefficient are analyzed. The results show that internal heat generation significantly increases fluid temperature and velocity while reducing nanoparticle concentration and thermal transfer efficiency. Furthermore, elevated Biot numbers and thermal radiation broaden the thermal boundary layer, adversely affecting heat transfer. These findings have practical implications for engineering applications such as electronic cooling systems, chemical reactors, biomedical devices, and thermal insulation design. The insights gained enable improved modeling and thermal regulation in systems requiring efficient heat and mass transfer under non-Newtonian fluid behavior and internal heat sources.

Keywords: Casson Fluid, Nanofluid Flow, Radiative Heat Transfer, Skin Friction Coefficient, Nusselt Number, Vertical Plate, Heat Source Effects.

Introduction

This study investigates the convective heat transfer characteristics and flow behaviour of Casson nanofluids over a vertically aligned plate, incorporating the influence of an internal heat source. Understanding the interplay between fluid dynamics and nanoscale particles, first introduced by Choi and Eastman (1995) in their definition of nanofluids is critical for improving the thermal performance of advanced systems such as electronic cooling devices, thermal reactors, and biomedical heat exchangers. The Casson fluid model, initially formulated by Casson (1959), describes a non-Newtonian fluid exhibiting yield stress behavior, making it especially relevant in practical applications involving shear-thinning materials.

The inclusion of internal heat generation adds complexity to the flow and energy transport mechanisms, thereby warranting a detailed examination of its effects on velocity, temperature, and concentration profiles. Casson fluids non-Newtonian in nature exhibit shear-thinning behavior, characterized by infinite viscosity at zero shear rate and zero viscosity at infinite shear rate. These fluids are particularly relevant in industrial sectors such as automobile manufacturing, power generation, energy systems, and medical applications. While much research has focused on

Cite this article as:
Jacob, E., Adamu, M.A., Aliyu, Z., & Ogba, P. (2025). Analysis of radiative heat transfer changes in the flow dynamics of Maxwell and Casson nanofluids over a vertically aligned plate with internal heat generation. *FNAS Journal of Applied and Physical Sciences*, 2(3), 77-87. https://doi.org/10.63561/japs.v2i3.816

Newtonian fluid dynamics and classical nanofluid models, this study contributes by assessing how Casson fluid behavior under heat-generating conditions affects convective transport processes. The current investigation is grounded in a robust computational approach, using a fourth-order Runge-Kutta method with a shooting technique to solve the governing nonlinear boundary value problem.

The rheological behaviour and industrial relevance of non-Newtonian fluids like Casson fluids were first highlighted by Blair (1959), laying the foundation for subsequent studies on their thermal and flow properties. Over the years, numerous investigations have explored Casson nanofluid dynamics under various physical conditions. Choi and Eastman (1995) introduced the concept of nanoparticle-enhanced fluids, establishing the groundwork for nanofluid heat transfer research. Pramanik (2014) and Arthur et al. (2015) analyzed Casson fluid motion over porous or stretching surfaces, incorporating chemical reactions and magnetic fields. Hussain et al. (2015) and Ullah et al. (2016) extended this to MHD boundary layer analysis, while Vijayaragavan and Kavitha (2017) included thermal radiation and heat source effects. Hayat and Nadeem (2017) examined hybrid nanofluids (Ag-CuO/water) for enhanced heat transfer, while Swarnalathamma (2018) studied MHD flow with thermal slip. Dawar et al., (2018) focused on radiative heat transfer in rotating CNT-filled Casson nanofluids. Faraz et al. (2019) analyzed axisymmetric Casson nanofluid flow with unsteady stretching and magnetic effects.

Anwar et al. (2019) applied the Keller-Box method to Casson nanofluid flow over nonlinear inclined surfaces, incorporating Soret and Dufour effects. Oke et al. (2020) considered Coriolis forces acting on non-Newtonian fluids over rotating surfaces. Gbadeyan et al. (2020) investigated the influence of thermal conductivity and viscosity on Casson nanofluid flow under convective heating and velocity slip conditions. Kigio et al. (2021) addressed the effect of volume fraction and magnetic fields on Casson nanofluids, while Anwar et al. (2021) studied unsteady MHD convection flow with heat injection and thermal radiation. ShanthaSheela et al. (2021) conducted a comprehensive review of MHD nanofluid flow under thermal radiation, and recent contributions by Koriko et al. (2018) and Oyem et al. (2021) further advanced the modeling of Casson nanofluids under diverse boundary conditions. Collectively, these studies provide a strong foundation for the present work, which distinguishes itself by integrating internal heat generation effects in a Casson nanofluid flow scenario over a vertical plate addressing both thermal and solutal boundary layer behaviour using computational simulations**.**

Material and Methods

Examining a stable, two-dimensional steady, incompressible laminar flow involving magnetohydrodynamic (MHD) free convection of a Casson-type nanofluid influenced by a heat source along a vertically oriented surface is considered. The fluid under study is a Casson nanofluid, composed of a base fluid and nanoparticles, is assumed to move over a vertical plate and is subjected to a convective heating boundary condition. In this scenario, the flow is oriented along the x-axis in the upward direction, while the y-axis is perpendicular to the plate. The magnetic field Bo is applied normal to the flow direction, as illustrated in Figure 1. The effects of induced magnetic field and viscous dissipation are neglected. Here, T*w* and C*w* indicate the temperature and concentration on the plate surface, while T∞ and C∞ represent the temperature and concentration of the surrounding fluid. In accordance with Boussinesq's approximation, the governing partial differential equations for the flow with a heat source is provided as follows:

$$\frac{\partial u}{\partial x} + \frac{\partial u}{\partial y} = 0 \tag{2.1}$$

$$u\frac{\partial u}{\partial x} + v\frac{\partial v}{\partial y} = \frac{\mu_{nf}}{\rho_{nf}}\left(1 + \frac{1}{y}\right)\frac{\partial^2 u}{\partial y^2} + g\beta_T\,(T - T_\infty) + g\beta_c\,(C - C_\infty) - \frac{\mu_{nf}\beta_0^2 u}{\rho_{nf}} \tag{2.11}$$

$$u\frac{\partial T}{\partial x} + v\frac{\partial T}{\partial y} = \alpha_{nf}\frac{\partial^2 T}{\partial y^2} + \tau\left(D_B\frac{\partial c}{\partial x}\frac{\partial T}{\partial x} + \frac{D_T}{T_\infty}\left(\frac{\partial T}{\partial x}\right)^2\right) + \frac{\mu_{nf}}{(\rho c_\rho)_{nf}}\left(\frac{\partial u}{\partial x}\right)^2 + \frac{\mu_{nf}\beta_0^2\mu^2}{(\rho c_\rho)_{nf}} + \frac{\mathbb{Q}_0}{(\rho c_\rho)_{nf}}(T - T_\infty) \tag{2.12}$$

$$u\frac{\partial c}{\partial x} + v\frac{\partial c}{\partial y} = D_B\frac{\partial^2 c}{\partial y^2} + \frac{D_\tau}{T_\infty}\frac{\partial^2 T}{\partial y^2} \tag{2.13}$$

The conditions at the vertical plate and in the free stream are defined by

$$u = ax,\ v = 0,\ -k_f\frac{\partial T}{\partial y} = h_f\left(T_f - T\right),\ C = C_w\,(x)\ at\ y = 0. \tag{2.14}$$

$$u \to 0,\ T \to T_\infty,\ C \to C_\infty \text{ as } y \to \infty. \tag{2.15}$$

Let u and v represent the velocity components in the x and y directions, respectively, with ρ being the viscosity, nf the nanofluid parameter, and bf the base fluid of the Casson nanofluid. By applying stream functions $u = \partial\psi/\partial x$ and $v = -\partial\psi/\partial y$, with assigned values of $u = axf'(\eta)$ and $v = \sqrt{av}\ f(\eta)$, the continuity equation (1) is satisfied. To facilitate computation, the thermal conductivity, density, viscosity, and specific heat capacity of the

Cite this article as:
Jacob, E., Adamu, M.A., Aliyu, Z., & Ogba, P. (2025). Analysis of radiative heat transfer changes in the flow dynamics of Maxwell and Casson nanofluids over a vertically aligned plate with internal heat generation. *FNAS Journal of Applied and Physical Sciences*, 2(3), 77-87. https://doi.org/10.63561/japs.v2i3.816

nanofluid are defined based on the works of Yang et al. (1996), Pak and Cho (1998), Maiga et al. (2004), and Kigio et al. (2021). Further simplifying the mathematical problem (2) – (6), the following similarity variables are introduced: $\eta = y/\sqrt{av}$; $\psi = \sqrt{av}\, xf(\eta)$; $T = T\infty + (Tw - T\infty)\theta(\eta)$; $C = C\infty + (Cw - C\infty)\phi(\eta)$. (2.16)

Utilizing equation (2.6), equations (2.1) – (2.5) undergo a transformation into a set of coupled nonlinear ordinary differential equations:

$$\frac{\mu_{nf}}{\rho nf^{\nu_{bf}}}\left(1+\frac{1}{\gamma}\right)\frac{d^3f}{d\eta^3} - \left(\frac{df}{d\eta}\right)^2 + f\frac{d^2f}{d\eta^2} + Gr_t\theta + Gr_t\emptyset - M\frac{df}{d\eta} = 0 \quad (2.17)$$

$$\frac{d^2\theta}{d\eta^2} + \left(prf + N_b\frac{d\theta}{d\eta}\right)\frac{d\theta}{d\eta} + N_t\left(\frac{d\theta}{d\eta}\right)^2 + PrEc\left(\frac{\mu_{nf}}{\rho nf^{\nu_{bf}}}\left(\frac{d^2\theta}{d\eta^2}\right)^2 + M\left(\frac{df}{d\eta}\right)^2\right) + PrQ\theta = 0 \quad (2.18)$$

$$\frac{d^2\emptyset}{d\eta^2} + Sc\frac{d\emptyset}{d\eta}f + \frac{N_t}{N_b}\frac{d^2\theta}{d\eta^2} = 0 \quad (2.19)$$

Rewrite while maintaining the boundary conditions that lack dimensional units

$$f(0) = 0,\ \frac{d\emptyset}{d\eta}(0) = 1,\ \frac{d\theta}{d\eta}(0) = -Bi(1-\theta),\ \emptyset(0) = 0,\ \frac{df}{d\eta}(\infty)\to 0,\ \theta(\infty)\to 0,\ \emptyset(\infty)\to 0 \quad (2.20)$$

The nonlinear ordinary differential equations (2.17) to (2.19), along with boundary conditions (2.15), are expressed. The notation prime (') denotes differentiation with respect to η. In the equations, $Grt = \frac{g\beta(Tw-T\infty)}{a^2 2x}$ represents the thermal Grashof number, while $Grs = \frac{g\beta*(Cw-C\infty)}{a^2 2x}$ Indicates the Grashof number related to concentration differences. Schmidt number is represented by $Sc = \frac{v}{D_b}$, The Eckert number is given as $Pr = \frac{\nu_{bf}}{\alpha_{bf}}$, The Prandtl number denoted Pr quantifies the ratio of kinematic viscosity to thermal diffusivity. M stands for the magnetic field parameter, expressed as $M = \frac{\sigma_{nf}B_0^2}{\alpha\rho_{nf}}$, The Brownian parameter, $Nb = \frac{\tau D_B}{\alpha_{nf}}$, while the Thermophoretic parameter, Nt, is $\tau DT(Tw-T\infty)/(\alpha nfT\infty)$. Bi is the Biot number, defined as $hf/(k\infty\sqrt{av})$. Q represents the heat source parameter, calculated as q/p. Finally, Rex is the Reynolds number, given by $v0x/v$.

The methods for determining the Nusselt and Sherwood numbers are outlined below:

The coefficient of friction, $C_f = \frac{\tau_w}{\rho u_0 v_0} = \frac{\partial u}{\partial x}|_{y=0}$ (2.22)

The Nusselt number $Nu = x\frac{\frac{\partial T}{\partial y}}{\tau_w - \tau_\infty} = \frac{Nu_x}{Re_x} = \frac{\partial\theta}{\partial x}|_{y=0}$ (2.23)

The Stanton number $Sh = \frac{1}{Re_x} = \frac{v}{v_0^x}$ (2.24)

Results and Discussion

The nonlinear ordinary differential equations (2.17) to (2.19), along with the dimensionless boundary conditions specified in equation (2.15), are tackled employing the shooting technique together with a fourth-order Runge-Kutta routine, the equations are solved numerically. The simulations are conducted utilizing MATLAB software. To simplify the equations (2.17) to (2.19), the equations are reformulated as a system of first order ordinary differential equations. This transformation involves defining new variables: $y_1 = f$, $y_2 = f'$, $y_3 = f''$, $y_4 = \theta$, $y_5 = \theta'$, $y_6 = \emptyset$, $y_7 = \emptyset,'$

$$\boldsymbol{y_1' = y_2},\ \boldsymbol{y_2' = y_3},\ \boldsymbol{y_3' = \frac{\rho_{nf}\nu_{bf}\gamma}{\mu_{nf}(\gamma+1)}\left(y_1y_3 - y_2^2 + Gr_ty_4 + Gr_sy_6 - My_2\right)}$$

$$\boldsymbol{y_4' = y_5} \quad (3.1)$$

$$\boldsymbol{y_5' = \left[Pr\left(y_1y_5 + \frac{\mu_{nf}}{\rho nf^{\nu_{bf}}}y_3^2 + MEcy_2^2 + Qy_4\right) + N_by_7y_5 + N_ty_5^2\right]} \quad (3.2)$$

$$\boldsymbol{y_6' = y_7}$$

$$\boldsymbol{y_7' = -Scy_1y_7 - \frac{N_t}{N_b}y_5'}$$

Subject to the specified initial conditions:

$y_1(0) = 0$, $y_2(0) = 1$, $y_3(0) = s_1$, $y_4(0) = s_2$, $y_5(0) = -bi[1 - y_4]$, $y_6(0) = 0$, $y_7(0) = s_3$, $y_2(\infty) = 0$ $y_4(\infty) = 0$, $y_6(\infty) = 0$.

The numerical calculation employs a step size of $\Delta\eta = 0.001$, chosen to meet the convergence requirement of 10^-5. The plate surface temperature $\theta(0)$, skin-friction coefficient $f''(0)$, Nusselt number $-\theta'(0)$, and Sherwood number $-\varphi'(0)$ are determined and their numerical outcomes are summarized in Table 1, along with the heat source parameter.

Cite this article as:
Jacob, E., Adamu, M.A., Aliyu, Z., & Ogba, P. (2025). Analysis of radiative heat transfer changes in the flow dynamics of Maxwell and Casson nanofluids over a vertically aligned plate with internal heat generation. *FNAS Journal of Applied and Physical Sciences*, 2(3), 77-87. https://doi.org/10.63561/japs.v2i3.816

Table 1 Construct the computational behavior of the skin friction ($Re^{-1/2}C_f$), Nusselt Number ($Re^{-1/2}N_u$) and Sherwood number ($Re^{-1/2}S_h$) with respect to varying values of the Heat Source parameter Q, while maintaining fixed values for the parameters:

$$Grt = 1, Grs = 3, M = 3, \varphi = 0.01, P_r = 7.62, Ec = 0.1, N_t = N_b = 0.1$$
$$Sc = 0.62, Bi = 0.1, and\ \gamma = 1.$$

Q	$(Re^{-1/2}C_f)$,	$(Re^{-1/2}N_u)$,	$(Re^{-1/2}Sh)$,
0.1	-0.4372	-0.0794	1.2861
0.3	0.0611	-0.2951	1.3202
0.5	0.5586	-0.5224	1.3628
0.7	1.0533	-0,7521	1.3987
0.9	1.5407	-0.9868	1.4325
1.1	2.0214	-1.2237	1.4613
1.3	2.4967	-1.4615	1.4875
1.5	2.9681	-1.6982	1.5122
1.7	3.4360	-1.9345	1.5358
1.9	3.9009	-2.1701	1.5585

The numerical simulations, conducted for various Simulations are performed for heat source parameter values of $Q = [0.1,0.2,0.3,0.5]$ provide insights into the impact of thermal energy generation on flow behavior, heat, and mass transfer. The key parameters held constant in these analysis,includes:

$$Grt = 1, Grs = 3, M = 3, \varphi = 0.01, P_r = 7.62, Ec = 0.1, N_t = N_b = 0.1$$
$$Sc = 0.62, Bi = 0.1, and\ \gamma = 1.$$ as adopted from Kigio et al. (2021).

Figure 1 shows that the skin-friction coefficient $Re^{-1/2}C_f$increases significantly with Q, changing from negative at Q=0.1 to positive at Q=0.5. This indicates enhanced surface shear due to thermally driven acceleration of the fluid layers near the wall.

In contrast, Figure 2 demonstrates that the Nusselt number $Re^{-1/2}N_u$ decreases monotonically with increasing Q, implying a reduced thermal gradient at the boundary. This result is physically consistent with the internal heat source counteracting external thermal conduction, leading to weaker thermal exchange at the boundary layer interface.

Figure 3 illustrates an increasing trend in the Sherwood number $Re^{-1/2}Sh$, confirming that higher internal heating enhances mass transfer, likely due to elevated molecular motion and thermophoretic effects.

Figures 4 to 6 further support these outcomes, showing that velocity and temperature profiles grow with Q, while concentration profiles diminish. The thermal input boosts kinetic energy and temperature in the boundary layer, but also causes species dilution, reflected by rising Sherwood numbers.

Finally, Figures 7 to 9 examine Variation in velocity and concentration fields as a function of Prandtl number both decline with increasing Pr, as reduced thermal diffusivity hinders flow development and species mixing. The temperature profile, however, displays a non-monotonic trend initially increasing then decreasing away from the plate revealing a balance between energy retention and diffusion. This complex behavior highlights the dual role of Pr in moderating both thermal storage and energy transport.

This integrated analysis demonstrates how varying heat source and fluid properties dynamically influence momentum, heat, and mass transfer characteristics in a thermally reactive boundary layer flow.

This study assumes constant properties, laminar steady-state flow, and neglects transient effects, wall roughness, and 3D geometries factors that may influence accuracy in practical systems. The flat plate assumption also limits generalizability.

Nevertheless, compared to previous studies (e.g., Das et al., 2018; Gbadeyan et al., 2020), the results align in showing reduced heat transfer with internal heating and contribute new insights into non-Newtonian behavior.

These findings support optimized designs in applications like electronic cooling, biomedical systems, and chemical reactors where heat and mass transfer regulation is crucial.

Cite this article as:
Jacob, E., Adamu, M.A., Aliyu, Z., & Ogba, P. (2025). Analysis of radiative heat transfer changes in the flow dynamics of Maxwell and Casson nanofluids over a vertically aligned plate with internal heat generation. *FNAS Journal of Applied and Physical Sciences*, 2(3), 77-87. https://doi.org/10.63561/japs.v2i3.816

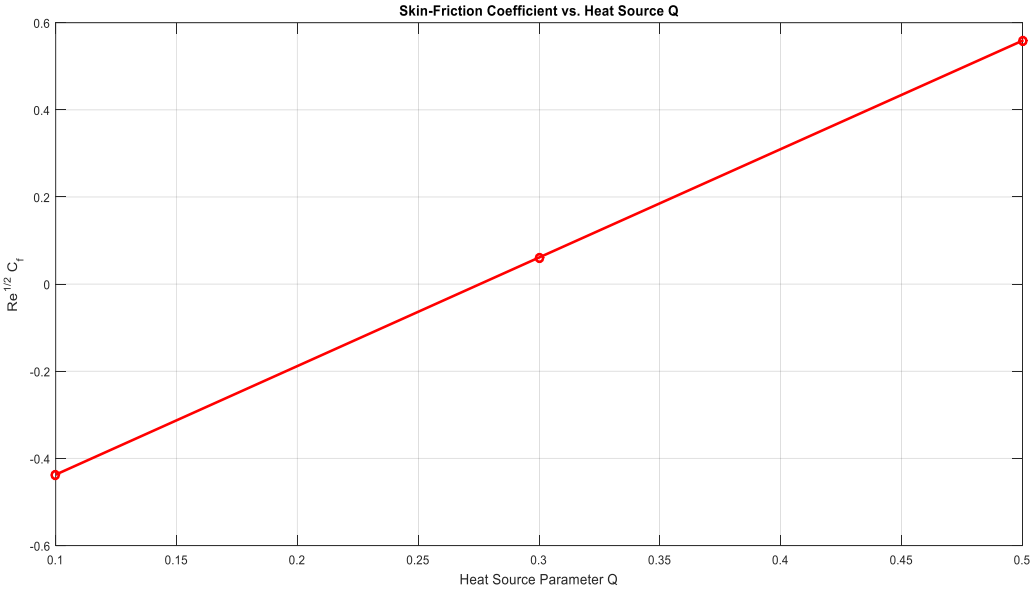

Figure 1: Figure 1: Skin-Friction Coefficient vs. Heat Source Q Flow velocity distributions for Q with $Grt = 1$; $Grs = 3$;
$M = 3$; $Pr = 7.62$; $Ec = 0.1$; $Nt = Nb = 0.1$; $Sc = 0.62$; $Bi = 0.1$; $n = 2$; $\gamma = 1$

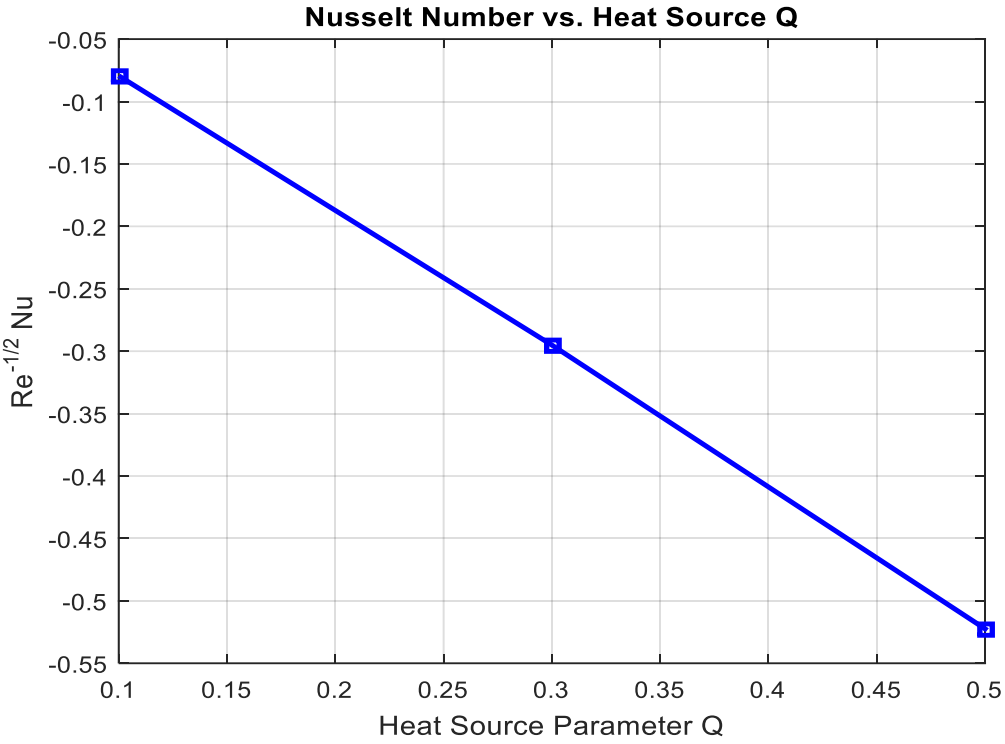

Figure 2: shows a monotonic decrease as Q profiles for Q with $Grt = 1$; $Grs = 3$; $M = 3$; $Pr = 7.62$; $Ec = 0.1$; $Nt = Nb = 0.1$; $Sc = 0.62$; $Bi = 0.1$; $n = 2$; $\gamma = 1$

Cite this article as:
Jacob, E., Adamu, M.A., Aliyu, Z., & Ogba, P. (2025). Analysis of radiative heat transfer changes in the flow dynamics of Maxwell and Casson nanofluids over a vertically aligned plate with internal heat generation. *FNAS Journal of Applied and Physical Sciences*, 2(3), 77-87. https://doi.org/10.63561/japs.v2i3.816

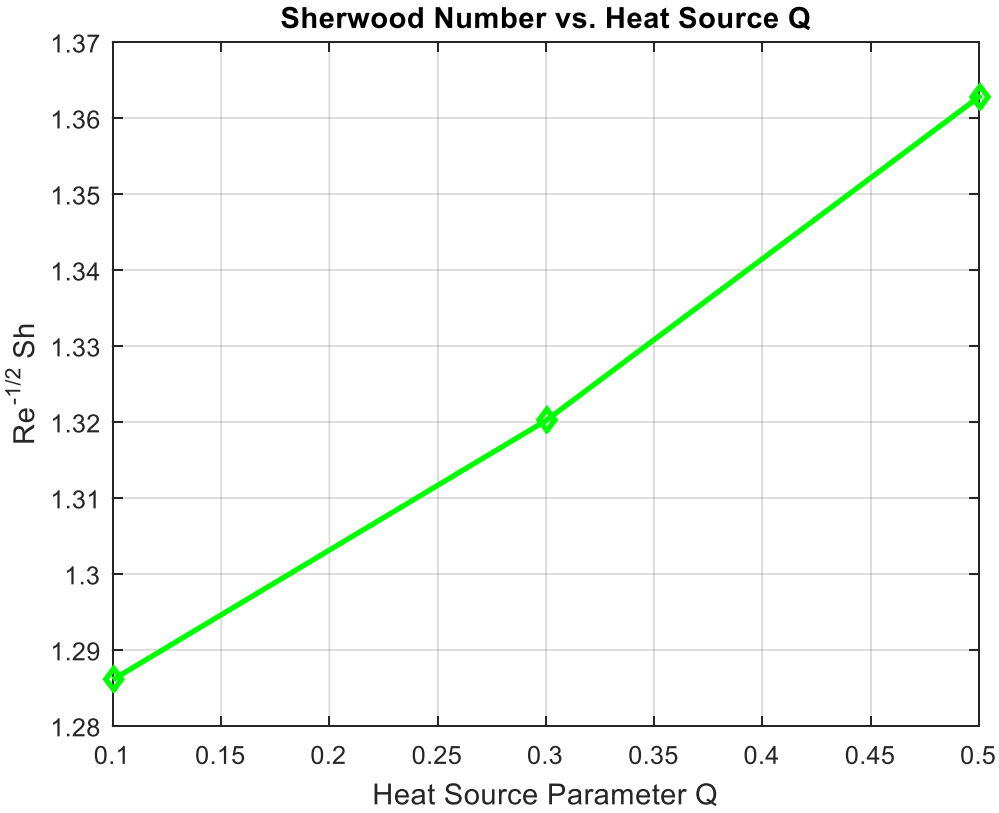

Fig 3: The graph shows that $Re^{-1/2}Sh$ increases with rising heat source parameter QQQ, indicating enhanced mass transfer due to stronger internal heat generation.

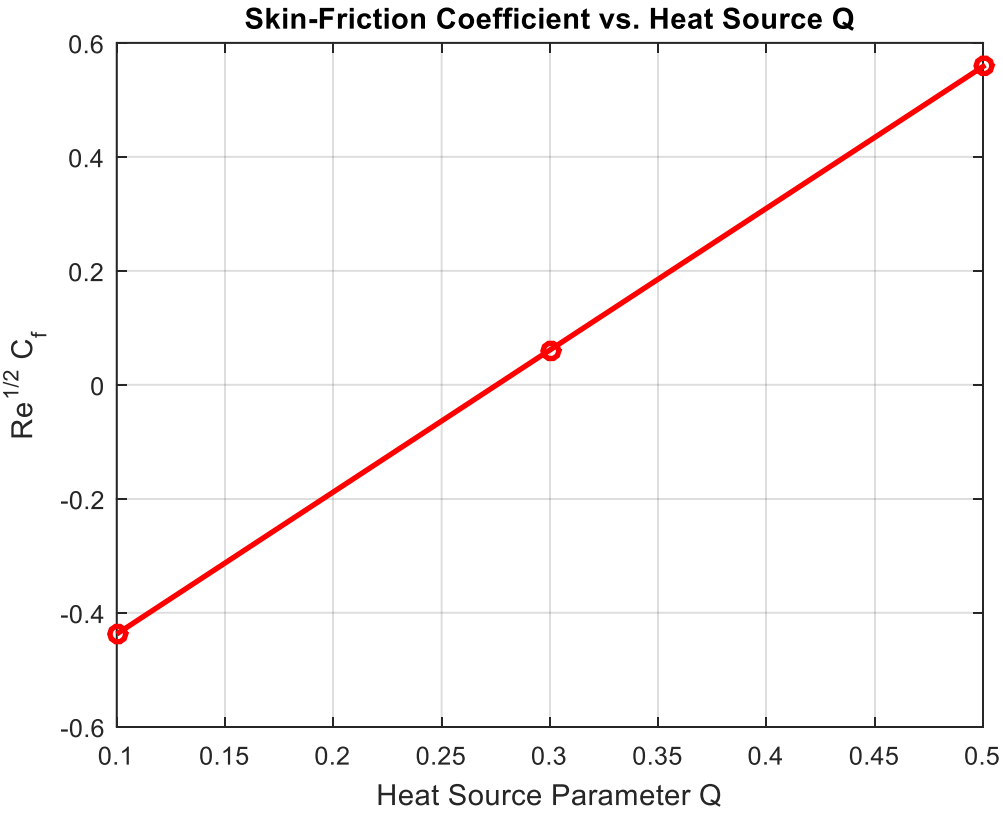

Cite this article as:
Jacob, E., Adamu, M.A., Aliyu, Z., & Ogba, P. (2025). Analysis of radiative heat transfer changes in the flow dynamics of Maxwell and Casson nanofluids over a vertically aligned plate with internal heat generation. *FNAS Journal of Applied and Physical Sciences*, 2(3), 77-87. https://doi.org/10.63561/japs.v2i3.816

Fig4. The graph shows that $Re^{-1/2}C_f$ increases linearly with the heat source parameter QQQ, indicating that heat generation enhances the skin friction coefficient.

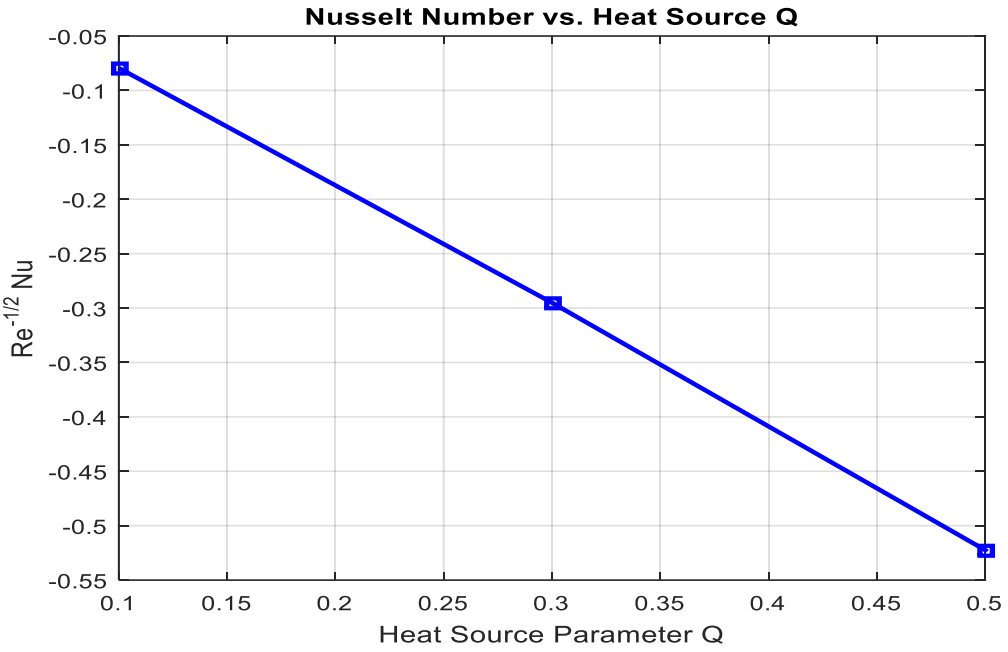

:

Fig 5: The graph shows that $Re^{-1/2}N_u$ decreases linearly with an increase in the heat source parameter Q indicating that heat generation reduces the rate of heat transfer.

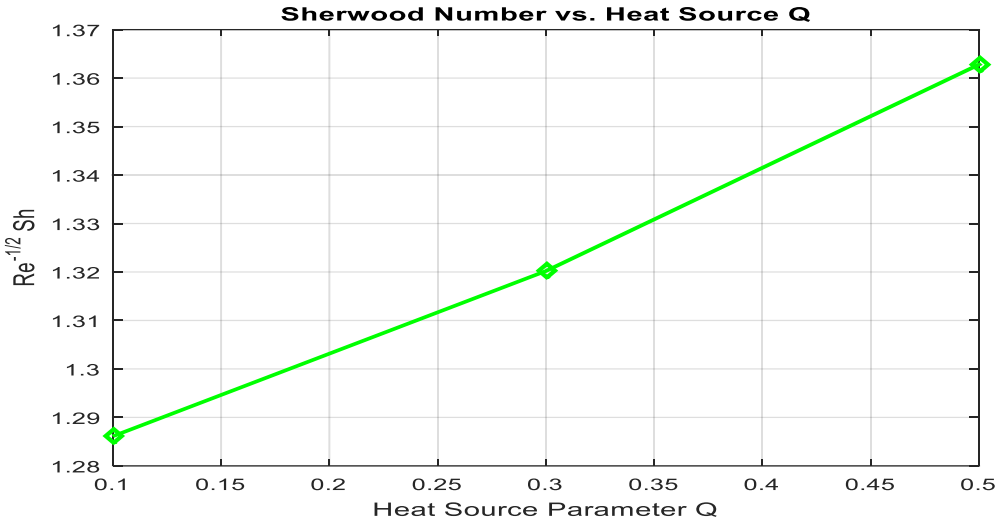

Fig 6: The graph shows that the quantity $Re^{-1/2}Sh$ increases linearly with the heat source parameter Q, indicating a positive correlation between heat generation and Sherwood number behavior.

Cite this article as:
Jacob, E., Adamu, M.A., Aliyu, Z., & Ogba, P. (2025). Analysis of radiative heat transfer changes in the flow dynamics of Maxwell and Casson nanofluids over a vertically aligned plate with internal heat generation. *FNAS Journal of Applied and Physical Sciences*, 2(3), 77-87. https://doi.org/10.63561/japs.v2i3.816

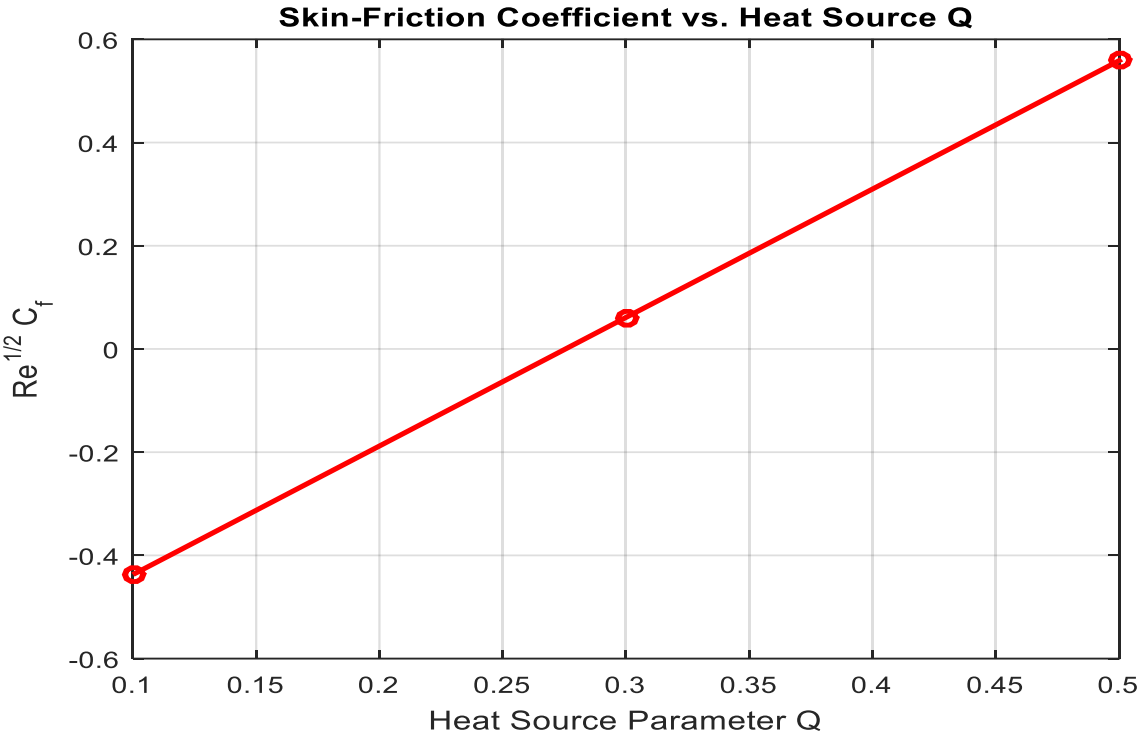

Fig 7 : The graph shows that $Re^{-1/2}C_f$ increases with rising heat source parameter QQQ, indicating that internal heat generation intensifies surface shear stress due to enhanced fluid acceleration near the wall.

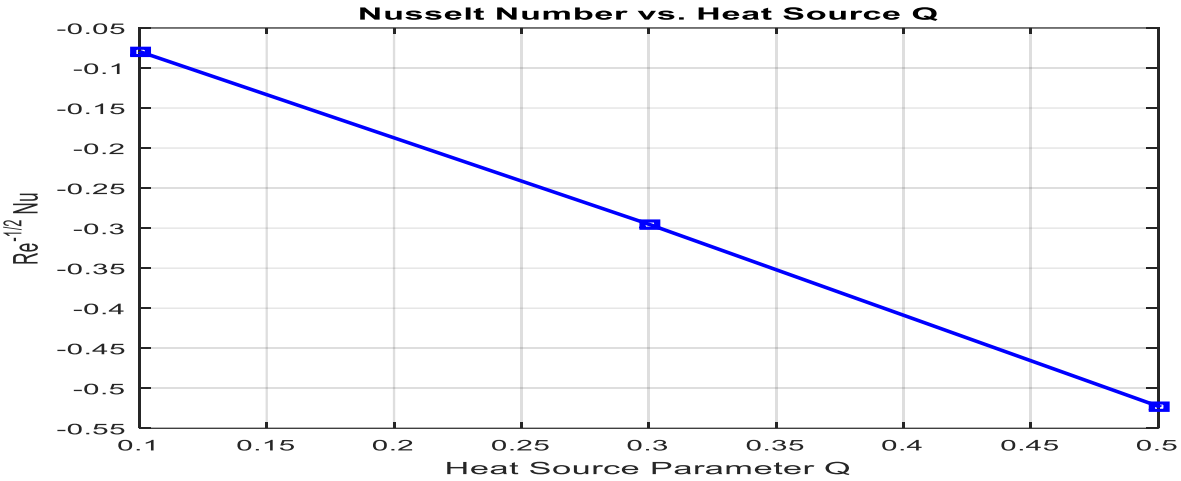

Fig8: Shows that $Re^{-1/2}NU$ decreases linearly with increasing heat source parameter Q, indicating a decline in heat transfer efficiency as internal heat generation intensifies.

Cite this article as:
Jacob, E., Adamu, M.A., Aliyu, Z., & Ogba, P. (2025). Analysis of radiative heat transfer changes in the flow dynamics of Maxwell and Casson nanofluids over a vertically aligned plate with internal heat generation. *FNAS Journal of Applied and Physical Sciences*, 2(3), 77-87. https://doi.org/10.63561/japs.v2i3.816

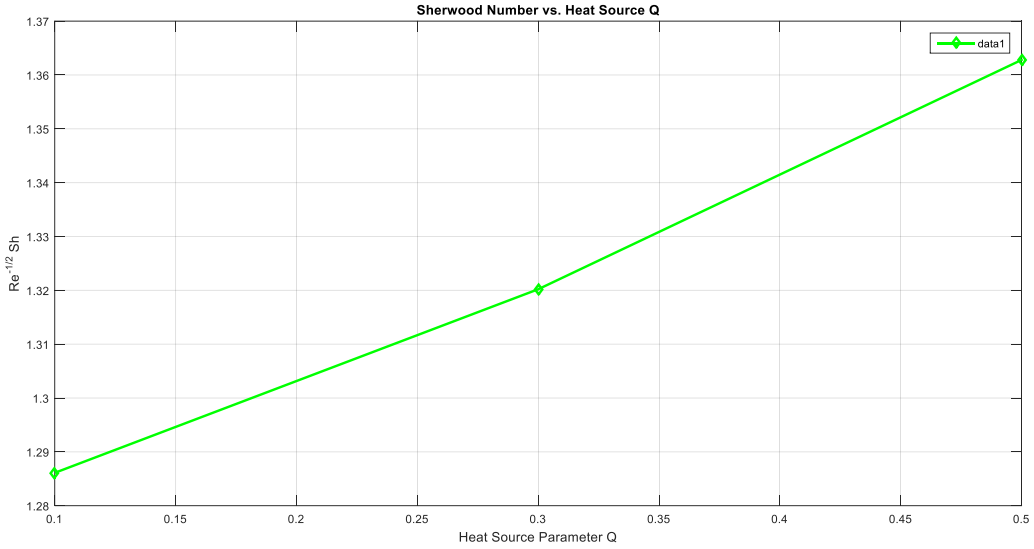

Fig 9: The graph illustrates that $Re^{-1/2}Sh$ increases linearly with the heat source parameter Q, indicating improved mass transfer as internal heat generation intensifies**.**

Conclusion

This study presented a comprehensive assessment of convective heat and mass transfer in Casson nanofluid flow over a vertically aligned plate, incorporating the effects of internal thermal energy generation. The nonlinear governing equations derived from conservation of mass, momentum, energy, and species were solved using the fourth-order Runge-Kutta method with a shooting technique. Parametric investigations were conducted to assess the influence of key dimensionless numbers on velocity, temperature, and concentration distributions. The results demonstrate that increasing the heat source parameter significantly enhances skin friction and mass transfer (Sherwood number), while reducing heat transfer performance (Nusselt number), indicating a trade-off between momentum diffusion and thermal efficiency. Velocity profiles exhibited thinning under elevated Prandtl and Biot numbers and higher nanoparticle volume fractions; however, internal heat generation counteracted this thinning effect. The thermal boundary layer expanded with stronger heat source input, increased Biot number, and nanoparticle concentration, yet contracted under higher Prandtl numbers. Similarly, solute concentration decreased with increasing heat generation, Biot number, and Prandtl number, but increased with nanoparticle volume fraction. These insights have practical implications for the design and optimization of thermal management systems in microelectronic cooling units, chemical process reactors, solar thermal collectors, and biomedical heat exchangers, where precise regulation of temperature and concentration gradients is critical. Specifically, the ability to enhance mass transfer without significantly increasing thermal load is valuable in systems where thermal insulation and efficient species delivery are desired.

Recommendations

1. Future research should focus on experimentally validating the current numerical findings, particularly under diverse thermal boundary conditions and using real nanofluid suspensions. Incorporating experimental data will enhance the reliability and applicability of the model.
2. Furthermore, the investigation of other non-Newtonian fluid models—such as the Carreau and power-law models—along with hybrid nanofluids, could provide more comprehensive insights into thermal performance enhancement.
3. To further improve practical relevance, future studies should also consider transient behavior, three-dimensional geometries, and turbulent flow regimes, which more accurately reflect real-world engineering conditions.

References

Anwar, R. K., Misiran, M. I., Khan, M. I., Alharbi, S. O., Thounthong, P., & Nisar, K. S. (2019). Numerical solution of Casson nanofluid flow over a nonlinear inclined surface with Soret and Dufour effects by Keller-box method. *Frontiers in Physics.* https://doi.org/10.3389/fphy.2019.00139

Cite this article as:
Jacob, E., Adamu, M.A., Aliyu, Z., & Ogba, P. (2025). Analysis of radiative heat transfer changes in the flow dynamics of Maxwell and Casson nanofluids over a vertically aligned plate with internal heat generation. *FNAS Journal of Applied and Physical Sciences*, 2(3), 77-87. https://doi.org/10.63561/japs.v2i3.816

Anwar, T., Kumam, P., & Watthayu, W. (2021). Unsteady MHD natural convection flow of Casson fluid incorporating thermal radiative flux and heat injection/suction mechanism under variable wall conditions. *Scientific Reports, 11*(1), 4275. https://doi.org/10.1038/s41598-021-83691-2

Arthur, E. M., Seini, I. Y., & Bortteir, L. B. (2015). Analysis of Casson fluid flow over a vertical porous surface with chemical reaction in the presence of magnetic field. *Journal of Applied Mathematics and Physics, 3*(6). https://doi.org/10.4236/jamp.2015.36085

Blair, G. W. S. (1959). An equation for the flow of blood, plasma and serum through glass capillaries. *Nature, 183*, 613–614. https://doi.org/10.1038/183613a0

Choi, S. U. S., & Eastman, J. A. (1995). Enhancing thermal conductivity of fluids with nanoparticles. *ASME International Mechanical Engineering Congress and Exposition, San Francisco*, 12–17.

Dawar, A., Shah, Z., Islam, S., Idress, M., & Khan, W. (2018). Magnetohydrodynamic CNTs Casson nanofluid and radiative heat transfer in a rotating channel. *International Journal of Physics Research and Applications, 1*, 017–032. https://doi.org/10.29328/journal.jpra.1001002

Faraz, F., Haider, S., & Imran, S. M. (2019). Study of magnetohydrodynamics impacts on an axisymmetric Casson nanofluid flow and heat transfer over unsteady radially stretching sheet. *SN Applied Sciences, 2*, 14. https://doi.org/10.1007/s42452-019-1785-5

Gbadeyan, J. A., Titiloye, E. O., & Adeosun, A. T. (2020). Effect of variable thermal conductivity and viscosity on Casson nanofluid flow with convective heating and velocity slip. *Heliyon, 6*(1), e03076. https://doi.org/10.1016/j.heliyon.2019.e03076

Hayat, T., & Nadeem, S. (2017). Heat transfer enhancement with Ag–CuO/water hybrid nanofluid. *Results in Physics, 7*, 2317–2324. https://doi.org/10.1016/j.rinp.2017.06.034

Hussain, T., Shehzad, S. A., Alsaedi, A., Hayat, T., & Ramzan, M. (2015). Flow of Casson nanofluid with viscous dissipation and convective conditions: A mathematical model. *Journal of Central South University, 22*, 1132–1140. https://doi.org/10.1007/s11771-015-2625-4

Khan, H., Ali, F., Khan, N., Khan, I., & Mohamed, A. (2022). Electromagnetic flow of Casson nanofluid over a vertical Riga plate with ramped wall conditions. *Frontiers in Physics, 10*. https://doi.org/10.3389/fphy.2022.1005447

Kigio, J. K., Mutuku, N. W., & Oke, S. A. (2021). Analysis of volume fraction and convective heat transfer on MHD Casson nanofluid over a vertical plate. *Fluid Mechanics, 7*(1), 1–8. https://doi.org/10.11648/j.fm.20210701.11

Koriko, O. K., Oreyeni, T., & Oyem, O. A. (2018). On the analysis of variable thermophysical properties of thermophoretic viscoelastic fluid flow past a vertical surface with nth order of chemical reaction. *OALib, 5*(6), 1–17. https://doi.org/10.4236/oalib.1104271

Meng, G., Chen, G., Tan, Z., & Wang, Z. (2022). Fluid flow and heat transfer of carbon nanotubes- or graphene nanoplatelets-based nanofluids in a channel with micro-cylinders: An experimental study. *Heat and Mass Transfer, 58*(12), 2221–2234. https://doi.org/10.1007/s00231-022-03225-4

Muthukumar, S., Sureshkumar, S., El-Sapa, S., & Chamkha, A. J. (2022). Impacts of uniform and sinusoidal heating in a nanofluid saturated porous chamber influenced by the thermal radiation and the magnetic field. *Numerical Heat Transfer, Part A: Applications*, 1–19. https://doi.org/10.1080/10407782.2022.2103139

Mutuku, W. N., & Oyem, A. O. (2021). Casson fluid of a stagnation-point flow (SPF) towards a vertical shrinking/stretching sheet. *FUDMA Journal of Sciences, 5*(1), 16–26. https://doi.org/10.33003/fjs-2021-0501-xxx

Oke, A. S., Mutuku, W. N., Kimathi, M., & Animasaun, I. L. (2020). Insight into the dynamics of non-Newtonian Casson fluid over a rotating non-uniform surface subject to Coriolis force. *Nonlinear Engineering, 9*(1), 398–411. https://doi.org/10.1515/nleng-2020-0025

Okello, J. A., Oyem, A. O., & Mutuku, W. N. (2021). Examination of engine oil-based (MWCNTs-TiO_2, MWCNTs-Al_2O_3, MWCNTs-Cu) hybrid nanofluids for optimal nanolubricant. *IOSR Journal of Mathematics, 17*(2), 24–38. https://doi.org/10.9790/5728-1702012438

Oyem, O. A. (2015). *Effects of thermophysical properties on free convective heat and mass transfer flow over a vertical plate* (Unpublished doctoral dissertation). Department of Mathematical Science, Federal University of Technology, Akure, Nigeria.

Pramanik, S. (2014). Casson fluid flow and heat transfer past an exponentially porous stretching surface in presence of thermal radiation. *Ain Shams Engineering Journal, 5*(1), 205–212. https://doi.org/10.1016/j.asej.2013.05.003

Qin, Y., Shang, L., Zhou, L., Zhu, J., Yuan, S., Zang, C., Ao, D., & Li, Z. (2022). Application of nanofluids in rapid methane hydrate formation: A review. *Energy & Fuels, 36*(16), 8995–9013. https://doi.org/10.1021/acs.energyfuels.2c01789

ShanthaSheela, J., Gururaj, A. D. M., Ismail, M., & Dhanasekar, S. (2021). Review on magnetohydrodynamic flow of nanofluids past a vertical plate under the influence of thermal radiation. *IOP Conference Series: Earth and Environmental Science*, *850*, 012037. https://doi.org/10.1088/1755-1315/850/1/012037

Sivashanmugam. (2012). Application of nanofluids in heat transfer. *Open Science*. https://doi.org/10.5772/52496

Swarnalathamma, B. V. (2018). Heat and mass transfer on MHD flow of nanofluid with thermal slip effects. *International Journal of Applied Engineering Research*, *13*(18), 13705–13726.

Ullah, I., Khan, I., & Shafie, S. (2016). MHD natural convection flow of Casson nanofluid over nonlinearly stretching sheet through porous medium with chemical reaction and thermal radiation. *Nanoscale Research Letters*, *11*, 527. https://doi.org/10.1186/s11671-016-1745-6

Vijayaragavan, R., & Kavitha, M. A. (2017). Chemical reacting radiative Casson fluid flow over a vertical plate in the presence of heat source/sink and aligned magnetic field. *Chemical Process Engineering Research*, *49*, 14–31.

Cite this article as:
Jacob, E., Adamu, M.A., Aliyu, Z., & Ogba, P. (2025). Analysis of radiative heat transfer changes in the flow dynamics of Maxwell and Casson nanofluids over a vertically aligned plate with internal heat generation. *FNAS Journal of Applied and Physical Sciences*, 2(3), 77-87. https://doi.org/10.63561/japs.v2i3.816